

Article

Metal Source and Fluid Evolution in Xiaojiashan Gold Deposit in Northeastern Hunan, China: Implications of Rare Earth Elements, Fluid Inclusions, and Pyrite S Isotopic Compositions

Dongzhuang Hou ^{1,*}, Shu Lin ^{2,3}, Lang Liu ⁴, Chao Huan ⁴ , Huaifu Qiu ⁴ and Bingbing Tu ⁵¹ College of Geology and Environment, Xi'an University of Science and Technology, Xi'an 710054, China² Second Mobile Corps of People's Armed Police, Fuzhou 350201, China³ School of Geosciences and Info-Physics, Central South University, Changsha 410083, China⁴ College of Energy Engineering, Xi'an University of Science and Technology, Xi'an 710054, China⁵ College of Sciences, Xi'an University of Science and Technology, Xi'an 710054, China

* Correspondence: hdz@xust.edu.cn

Abstract: The material source and the evolution of ore-forming hydrothermal fluids of Xiaojiashan gold deposits remain controversial. We carried out a mineralogical characteristics analysis, trace elements analysis, sulfur isotope composition analysis, and fluid inclusion microthermometry in order to explore the ore-forming sources, conditions, and process of this deposit. Gold mineralization can be divided into three stages: the quartz-pyrite stage, the quartz-polymetallic sulfide stage, and the quartz-ankerite stage. This gold deposit was probably formed under the following conditions: temperature of 122–343 °C and salinity of 0.8–11.4 wt% (NaCl). It was inferred that the ore-forming hydrothermal fluids were early metamorphic–hydrothermal (Stage I) and late magmatic–hydrothermal (Stages II and III), and were characterized by medium–low temperature and medium–low salinity based on fluid inclusion microthermometry and S isotope composition. The temperature and salinity of the ore-forming fluid decreased during mineralization, which was caused by the involvement of groundwater. The chondrite-normalized trace element patterns of the gold ores are similar to the host rocks of the Lengjiayi Formation, indicating that the ore-forming materials were sourced from the Lengjiayi Formation. The S isotopes indicated that the magmatic components also provided the ore-forming materials during Stages II and III.

Keywords: metallogenic condition; vein-hosted gold; fluid evolution; fluid inclusion; Xiaojiashan gold deposit



Citation: Hou, D.; Lin, S.; Liu, L.; Huan, C.; Qiu, H.; Tu, B. Metal Source and Fluid Evolution in Xiaojiashan Gold Deposit in Northeastern Hunan, China: Implications of Rare Earth Elements, Fluid Inclusions, and Pyrite S Isotopic Compositions. *Minerals* **2023**, *13*, 121. <https://doi.org/10.3390/min13010121>

Academic Editor: Jan Marten Huizenga

Received: 16 November 2022

Revised: 8 January 2023

Accepted: 11 January 2023

Published: 13 January 2023



Copyright: © 2023 by the authors. Licensee MDPI, Basel, Switzerland. This article is an open access article distributed under the terms and conditions of the Creative Commons Attribution (CC BY) license (<https://creativecommons.org/licenses/by/4.0/>).

1. Introduction

The source of ore-forming materials and the evolution of ore-forming fluids are the basis for the investigation of the genesis of deposits and establishing metallogenic mechanisms. Due to the stability, similarity, and differentiation of rare earth elements (REEs), the geochemistry of rocks has been adopted to determine fluid–rock interactions, protolith restoration, and the genesis of minerals [1,2]. The isotopic composition of S ($\delta^{34}\text{S}$) in sulfide ore minerals may provide information about their origin [3]. Fluid inclusions entrapped in minerals formed during mineralization are actual samples of paleo-geofluids, providing indispensable information about the mineral formation environments and geologic processes in which the minerals were formed [4,5].

The Qinzhong–Hangzhou metallogenic belt, located at the suture zone between the Yangtze block and the Cathaysia block (Figure 1a) [6–8], is one of the most widely known belts in China. Northeastern Hunan, an important part of the Qinzhong–Hangzhou metallogenic belt, hosts more than 250 gold deposits (occurrences) with similar occurrence rates, ore-bearing strata, and geological characteristics [9–12]. Various models have been proposed for their genesis, including orogenic [13–15], epithermal [16], intrusion-related [4,17],

superimposed reformation [18], and SEDEX types [19,20]. One of the key controversies is the source of ore-forming materials and fluids. Liu et al. [21] proposed that the gold came from the Lengjiayi Group. However, Dong et al. [22] and Xu et al. [13] argued that the gold was from the mixed sources of the Lengjiayi Group, as well as mantle or deep crust magmatic rock.

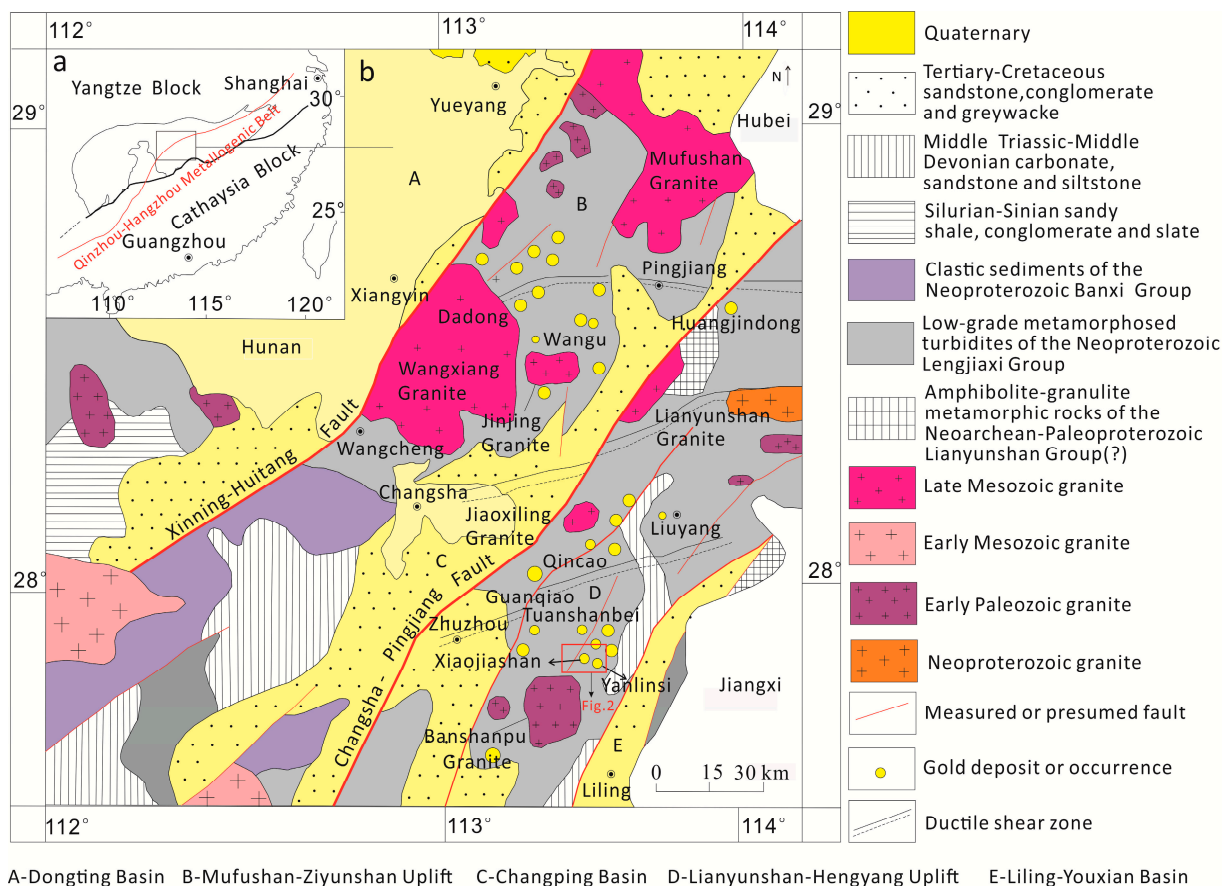


Figure 1. Geological map of the region showing distribution of gold deposits. (a) Simplified tectonic map of Qinzhou-Hangzhou mineralization belt. (b) Sketched geological map of northeastern Hunan (modified after [13]).

The Xiaojiashan gold deposit (reserve: 7.77 t, grade: 2.88 g/t [23]) is located in the Qinzhou-Hangzhou metallogenic belt (Figure 1b), and is thought to have great prospecting potential. Intense studies have thus been carried out on its geological features [24–26], ore-forming material sources [18,27,28], and fluid inclusions [29,30]. However, the published results are controversial in terms of the ore-forming fluids. Tao et al. [29] proposed that the ore-forming fluids comprised metamorphic hydrothermal water with superimposed magmatic-hydrothermal water and, later, groundwater. However, Lin [30] argued that the ore-forming fluids were mainly magmatic water. A further study, by Tan et al. [18], suggested a distinct shift of ore-forming fluids from metamorphic to magmatic water during early- and late-stage mineralization, respectively, by studying the trace element compositions and sulfur isotopes of pyrite. Therefore, detailed work on field geological investigations and petrological characteristics, trace element compositions, sulfur isotopic compositions and fluid inclusions of different-mineralization-stage gold ores was carried out. The aim was to provide some new insights to probe into the gold source, metallogenic condition, and fluid evolution of gold mineralization of the Xiaojiashan gold deposit and support future geological exploration and prediction.

2. Regional Geology

Northeastern Hunan is one of the vital gold metallogenic regions in Hunan Province, central Qinzhou–Hangzhou (Qin–Hang) metallongenic belt [31]. Yanlinsi, Xiaojiashan, Huangsikeng, Zhengchong, Haizichong, etc., have all been discovered in this area (Figure 2). The strata exposed in the region comprise a Neoproterozoic Lengjiayi Group of epimetamorphic lithic sandstone, slate, and silty slate, along with volcanic tuffaceous materials, Upper Paleozoic carbonate rocks, and Mesozoic–Cenozoic clastic rocks [9,12–16]. Furthermore, the Lengjiayi group is thought to be closely related to gold mineralization.

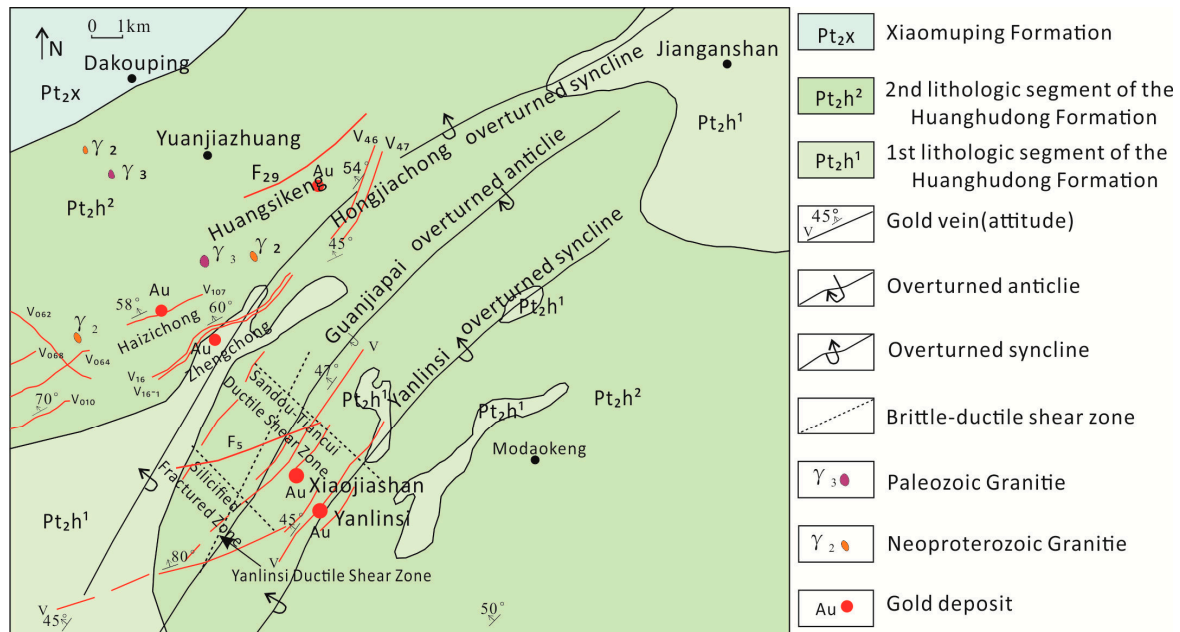


Figure 2. Schematic geological map of the Xiaojiashan deposit.

The tectonic lines are mainly composed of nearly NE-trending abyssal faults of Xinning–Huitang, Changsha–Pingjiang and Liuyang–Liheng from west to east, as well as pervasively developed folds [13,32]. The Changsha–Pingjiang fault in northeastern Hunan was an active fault with gold deposits (occurrences) (Figure 1b). Ore occurrences were manipulated by NE-trending subsidiary faults, folds, and shear zones [21,33].

Magmatic activity has occurred several times and magmatic rocks have developed from the Wuling orogeny to Yanshanian. Daweishan granite (802 Ma) was formed during the Neoproterozoic [34], Banshanpu granites (423–421 Ma) were formed during the early Paleozoic [35], and Lianyunshan granites (149 ± 1 Ma) were formed during the late Mesozoic [36].

3. Deposit Geology

The exposed strata in the deposit are the Huanghudong Formation and Xiaomuping Formation of the Lengjiayi Group in the Neoproterozoic. The Huanghudong Formation, the ore-hosting strata for the gold deposits, is dominated by quartz graywacke, siltstone, and slate (Figure 3a), whereas the Xiaomuping Formation consists mainly of slate, silty slate, and sericite slate. The folds and faults are well developed and the tectonic lines are mainly NE and NW. The faults include F₃, F₅, F₂₉, the Sandou–Tiancui ductile shear zone, the Yanlinsi ductile shear zone (Figure 2), and a silicified fractured zone. In the middle of the ductile shear zones, there is a flow cleavage, with a tectonic lenticular zone and a cleavage zone on both sides. The fold tectonics are known as Hongjiachong overturned syncline, Guanjiapai overturned anticline, and Yanlinsi overturned syncline from north to south. In the Yanlinsi and Haizichong gold deposits, there are only small plutons; larger, concealed

plutons are present in the NE direction of Banshanpu granite, according to remote-sensing images, gravity, and magnetic anomalies [37].

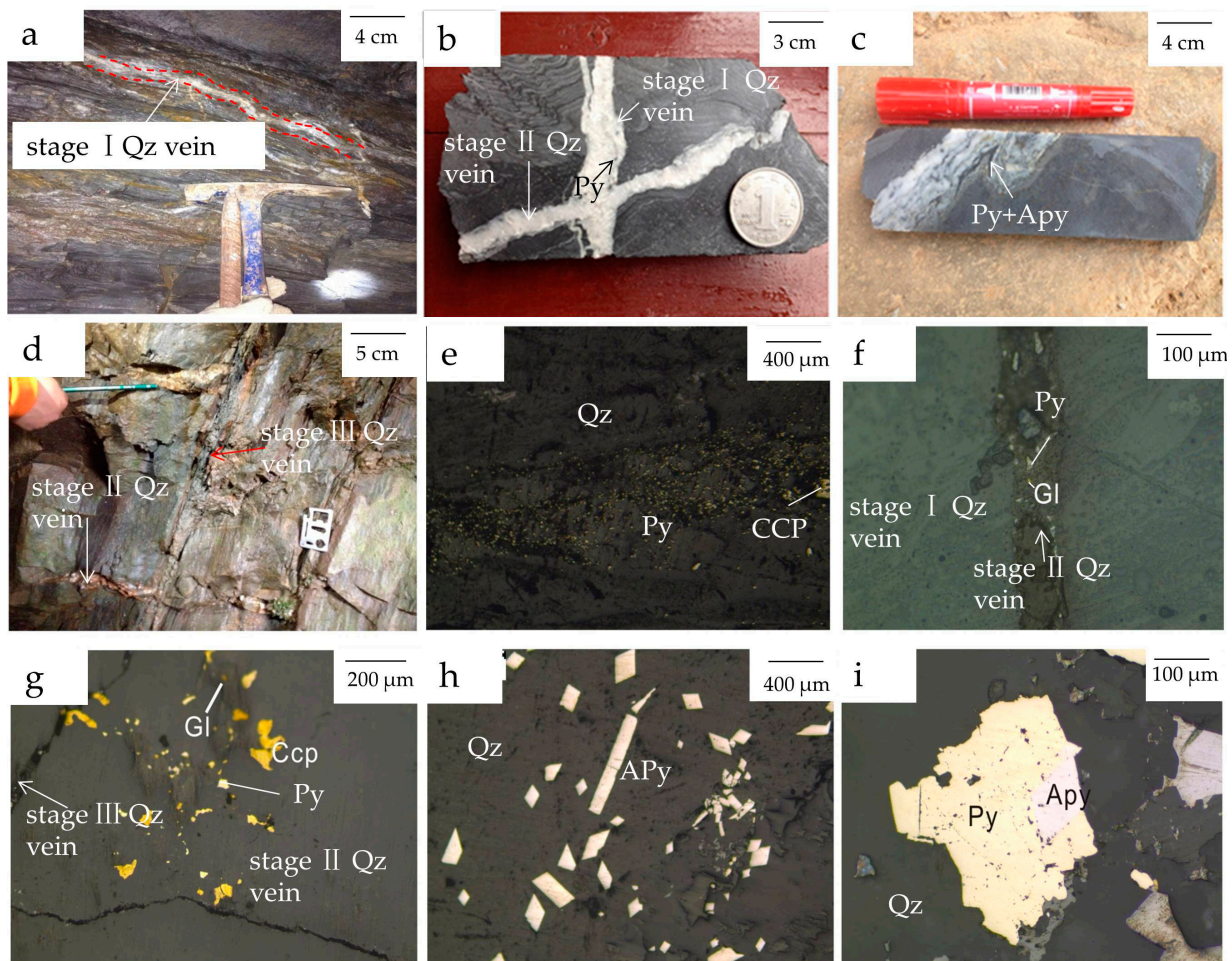


Figure 3. Ore features and photomicrographs of Xiaojiashan gold deposit. (a) Stage I smoky-gray quartz veins and alteration halo. (b) Stage II quartz vein cut stage I quartz vein. (c) Stage II sinuous smoky-gray quartz vein and alteration halo with disseminated pyrite and arsenopyrite. (d) Stage III quartz vein cut stage II quartz vein. (e) Silicic alterations with disseminated pyrite and arsenopyrite related to gold mineralization. (f) Stage II quartz vein overprinted stage I quartz vein. (g) Stage III quartz vein overprinted stage II quartz vein. (h) Silicic alterations with disseminated arsenopyrite related to gold mineralization in stage II. (i) Pyritization alterations with disseminated arsenopyrite related to gold mineralization in stage II. Abbreviations: Apy, Arsenopyrite; Ccp, Chalcopyrite; Gl, Gold; Py, Pyrite; Qz, Quartz; Sp, Sphalerite.

The Xiaojiashan gold deposit consists of 46 orebodies, most of which occur as NE-trending veins/veinlets with a dip of 30–60° in the strata and cleavage zones in the core of the overturned anticline. The orebodies are 250–500 m long and 0.38–3.30 m wide, with a gold grade of 0.25–14.84 g/t. The gold ore is quartz-vein-type and is composed primarily of pyrite and arsenopyrite, with smaller amounts of chalcopyrite, galena, sphalerite, and gold (Figure 3b–i). The gangue minerals include quartz, sericite, calcite, and chlorite. The gold usually occurs as micro-gold and fissure gold with inclusion and intergranular gold in rather low amounts. There are two types of opal quartz vein: one with a lower quantity of gold and another with black bands (Figure 3c). Gold contents depend on the band amounts: the more black bands, the higher the grade of the gold in the veins. These black-banded quartz veins also contain pyrite, arsenopyrite, galena, and sphalerite. The primary ore structures include the anhedral–subhedral structure, xenomorphic granular structure,

metasomatic structure, solid-solution-separation structure, poikilitic structure, etc. The ore structures mainly comprise massive structure, disseminated structure, veined-network structure, and stripe structure with gold enrichment.

Hosted rock alterations mainly include silicification, pyritization, sericitization, chloritization, and carbonation. Among these alterations, silicification and pyritization are closely associated with gold mineralization. Pyrite is an important gold-bearing mineral (Figure 3f,g) consisting of coarse- and fine-grained pyrite distinguished by degrees of crystallization. Coarse-grained pyrite, formed in the early stage of hydrothermal metallogenesis, is dark-yellow-colored, highly euhedral and poorly gold-bearing. By contrast, fine-grained pyrite, formed in the middle and late stages of hydrothermal metallogenesis, is light-yellow-colored, mainly subhedral-hypidiomorphic, and rich in gold.

Based on investigations of the veins carried out during fieldwork and from ore photomicrographs (Figure 3a–i), the metallogenic period can be divided into three stages. Stage I can be regarded as the quartz–pyrite stage, with quartz and coarse-grained pyrite formed and with weak gold mineralization. Stage II is the quartz–polymetallic sulfide stage, with quartz, pyrite, arsenopyrite, sphalerite, galena, chalcopyrite, and gold, as well as a minor amount of ankerite (Figure 3c). The quartz veins have black bands and the grain size of the quartz decreases (Figure 3e–i). Furthermore, the pyrite is mostly in a subhedral granular structure (Figure 3e,g,i), and most of the arsenopyrite is acicular and arranged in long columns (Figure 3h). The structure of the arsenopyrite is mainly automorphic in the early stage, while that in the late stage is generally semi-self-shaped and fine-grained. The arsenopyrite-metasomatized pyrite can be observed under the microscope (Figure 3i). The degree of gold mineralization is higher in Stage II. Quartz, ankerite, and pyrite in minor amounts are formed during Stage III, which is then known as the quartz–ankerite stage. Veins which are ore-barren are commonly cut Stage II veins (Figure 3d). The paragenetic sequence is illustrated in Figure 4.

	Stage I	Stage II	Stage III
Quartz	—————	—————	—————
Pyrite	—————	—————	—————
Arsenopyrite		—————	
Chalcopyrite		—————	
Sphalerite		—————	
Gold		—————	
Ankerite	—————		—————

Figure 4. Mineral paragenetic sequence for the Xiaojiashan gold deposit.

4. Sampling and Analytical Methods

Eighteen and sixteen samples were obtained from four drill holes and an exploration tunnel, respectively, during the field geological investigation of the present work. The sampling information and analysis methods are presented in Table 1.

4.1. Trace Element Analysis

In order to identify sources of gold, samples were grained to 74 μm . Trace elements in samples from veins and hosted rocks of the main metallogenic stages were analyzed by ICP-MS at Beijing Research Institute of Uranium Geology with an analytical precision of around 1%.

4.2. Sulfur Isotope Analysis

The observations from the fieldwork and photomicrographic study indicated that the pyrite was the foremost gold-bearing mineral. Samples of the pyrite from the quartz veins at different metallogenic stages were thus selected for sulfur isotope analysis. This

was performed using the direct-oxidation method using a MAT 253 mass spectrometer. The analysis was conducted at the Beijing Research Institute of Uranium Geology with an analytical precision of $\pm 0.2\%$.

Table 1. Analyses and sampling localities.

	Lithology	Sampling Position	Stage	Testing
X1	Quartz associated with pyrite quartz	Drillhole	Stage I	Trace, S isotope, Temperature
X2		Exploration tunnel		Trace, Temperature
X3	Quartz associated with sulfide	Drillhole	Stage II	Trace, S isotope, Temperature
X5	Quartz associated with pyrite	Drillhole		Trace, S isotope, Temperature
X7	Quartz associated with sulfide	Exploration tunnel		Trace, S isotope, Temperature
X8	Quartz associated with sulfide	Exploration tunnel		Temperature
X9	Quartz associated with sulfide	Exploration tunnel		Temperature
X10	Quartz associated with pyrite	Drillhole	Stage III	Trace, S isotope, Temperature
X11	Quartz associated with ankerite	Exploration tunnel		Trace, S isotope, Temperature
X12	Quartz associated with ankerite	Exploration tunnel		Temperature
X4	Sericite slate (X5 hanging -wall)	Drillhole	Hosted rock	Trace
X6	Sandy slate (X5 foot -wall)	Drillhole		Trace

4.3. Fluid Inclusions Microthermometry

To explore the metallogenic conditions at different mineralization stages, fluid inclusion microthermometry was performed in quartz samples using a Linkam THMS-600 microthermometer at the Key Laboratory of Non-ferrous Metallogenic Prognosis, Ministry of Education, School of Geosciences and Information Physics, Central South University. Before the measurements were made, the samples were double-side polished to a thickness of 0.06–0.08 mm. The instrument was calibrated with synthetic inclusion (international standard sample) before testing. The measuring range was from -196 to 600 °C. Uncertainties of the measurements were ± 0.1 °C and ± 1 °C in temperature ranges of <30 °C and <600 °C, respectively. The heating/freezing rate was 10 – 20 °C/min during the initial runs, which was reduced to 0.2 °C/min near the phase transformation.

5. Results

5.1. Trace Element Geochemistry

Table 2 shows that the total amount of rare earth elements (REEs) was 72.62–198.83 ppm, with the contents of light rare earth elements (LREEs) and Heavy rare earth elements (HREEs) ranging from 64.73–171.35 ppm and 7.89–27.48 ppm, respectively. The LREE/HREE, $La_{(N)}/Sm_{(N)}$, and $Gd_{(N)}/Yb_{(N)}$ ratios were 6.24–11.58, 2.03–4.68, and 1.43–2.96, respectively, indicating an enrichment of LREEs and a depletion of HREEs. Most of the samples displayed moderately negative Eu anomalies and no Ce anomalies (Figure 4). The REE content of the ores during Stage III was significantly lower than that in the Stage I and II ores, however, no significant differences were identified for the other elements.

As depicted in Figure 5, the REE profiles of both the hosted rocks (X4 and X6) and the ore were right-inclined and nearly parallel. The values of LREE/HREE, $La_{(N)}/Sm_{(N)}$, $Gd_{(N)}/Yb_{(N)}$, δEu , and δCe for the samples of hosted rock were similar to those of the ore samples. The samples of the rocks and ore were characterized by enrichment in LREE, depletion in HREE, and non-anomalies in Ce. The primitive mantle-normalized trace element distribution patterns of the ore and hosted rocks were right-inclined (Figure 6). The high field strength element (HFSE) was relatively depleted, especially in Nb and Ta. However, the large ion lithophile element (LILE) was enriched with Pb, displaying a positive anomaly.

Table 2. Trace element contents (ppm) and parameters in Xiaojiashan gold deposit.

	X1	X2	X3	X4	X5	X6	X7	X10	X11
V	22	93	64	117	120	86	7	13	15
Cr	90	90	70	80	90	70	90	90	110
Co	3.7	13.2	7.9	6.9	15.8	9.3	2.0	2.5	3.1
Ni	17.7	27.0	19.2	17.2	35.9	22.6	5.0	8.4	8.5
Cu	27.8	7.4	20.4	38.2	36.4	42.3	6.7	120.5	175.0
Zn	33	114	39	96	95	89	35	760	332
As	2120	88.8	161.5	4370	64.7	228	3700	4170	9350
Rb	26.4	150.0	109.0	246	185.0	143.0	17.0	21.5	27.4
Sr	170.0	155.0	116.5	58.5	120.0	130.0	10.8	90.7	45.9
P	210	1290	410	470	580	560	100	800	40
Y	6.7	13.6	10.1	11.3	10.9	11.5	1.0	4.2	2.2
Zr	67.5	148.0	105.5	171.5	138.5	117.0	12.3	16.9	21.5
Nb	2.5	11.2	8.1	6.1	10.3	9.5	0.9	1.3	2.0
Sb	29.3	2.64	3.87	5.85	4.00	9.85	8.77	72.7	78.8
Cs	2.68	8.99	5.93	15.45	11.05	7.79	1.24	1.29	1.56
Ba	90	560	320	640	570	360	40	50	70
La	14.3	30.9	29.1	33.5	33.1	28.1	2.7	4.9	6.0
Ce	29.3	71.1	62.8	74.9	72.6	61.0	5.79	11.85	13.25
Pr	3.33	9.19	7.66	8.70	8.62	7.18	0.62	1.60	1.49
Nd	12.5	34.8	28.2	32.0	31.9	27.0	2.4	6.6	5.5
Sm	2.75	7.55	5.77	6.46	6.91	5.71	0.40	1.94	1.01
Eu	0.65	1.71	1.18	1.27	1.30	1.12	0.14	0.84	0.19
Gd	2.58	7.73	4.79	6.27	5.92	5.36	0.32	1.86	0.78
Tb	0.36	1.17	0.67	0.92	0.85	0.80	0.03	0.22	0.09
Dy	2.09	7.32	4.33	6.11	5.53	4.85	0.28	1.12	0.69
Ho	0.41	1.53	0.91	1.23	1.15	1.03	0.06	0.24	0.15
Er	1.14	4.26	2.46	3.87	3.19	2.96	0.15	0.54	0.42
Tm	0.14	0.62	0.35	0.55	0.48	0.44	0.02	0.07	0.06
Yb	1.02	4.22	2.52	3.37	3.07	2.89	0.18	0.52	0.45
Lu	0.15	0.63	0.37	0.51	0.47	0.44	0.01	0.07	0.05
Hf	1.8	6.5	5.0	5.4	5.1	4.9	0.4	0.6	0.7
Ta	0.3	1.0	0.8	1.0	1.1	0.9	0.1	0.1	0.2
Au	0.775	0.074	0.012	0.587	0.007	0.09	4.12	6.08	10
Pb	61.7	24.6	13.8	12.5	26.8	31.7	441	1525	459
Th	4.9	12.5	10.6	15.1	14.8	12.6	1.0	1.7	2.0
U	2.4	2.5	2.3	2.8	3.2	2.4	0.3	0.5	0.6
ΣREE	72.62	198.83	159.21	180.76	182.99	153.48	13.21	35.22	31.38
LREE	64.73	171.35	142.81	157.93	162.33	134.71	12.16	30.58	28.69
HREE	7.89	27.48	16.4	22.83	20.66	18.77	1.05	4.64	2.69
LREE/HREE	8.2	6.24	8.71	6.92	7.86	7.18	11.58	6.59	10.67
La _(N) /Yb _(N)	10.83	6.34	9.25	7.47	8.53	7.5	11.56	8.41	10.84
δEu	0.73	0.68	0.67	0.6	0.61	0.61	1.16	1.33	0.63
δCe	0.98	1.04	1.01	1.01	1.03	1.02	0.99	1.04	1.01
La _(N) /Sm _(N)	3.62	3.19	3.64	3.51	3.41	3.41	4.68	2.03	4.35
Gd _(N) /Yb _(N)	2.09	1.52	1.57	1.54	1.6	1.53	1.47	2.96	1.43

The standard reference value of the rare earth element is C1-cyhalite as measured by [38].

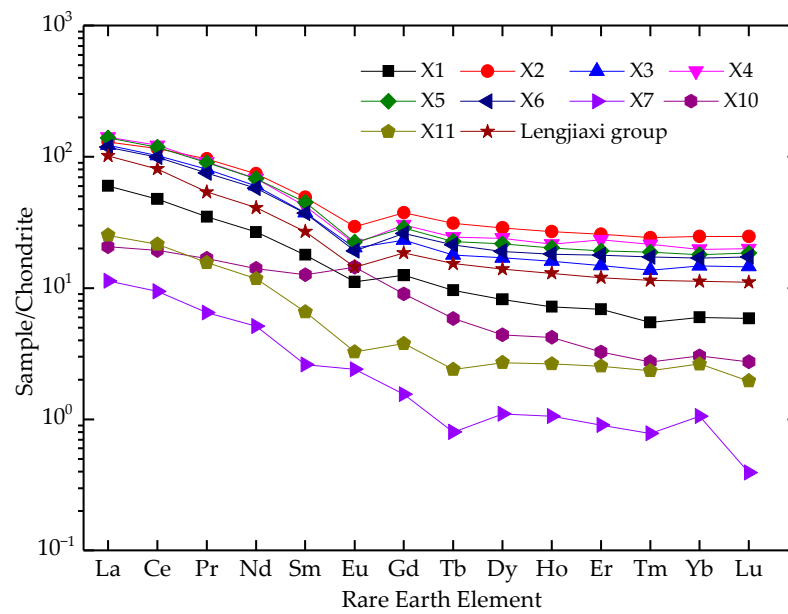


Figure 5. Chondrite-normalized REE distribution patterns of hosted rocks and ore. (Lengjiaxi Group modified after [39]).

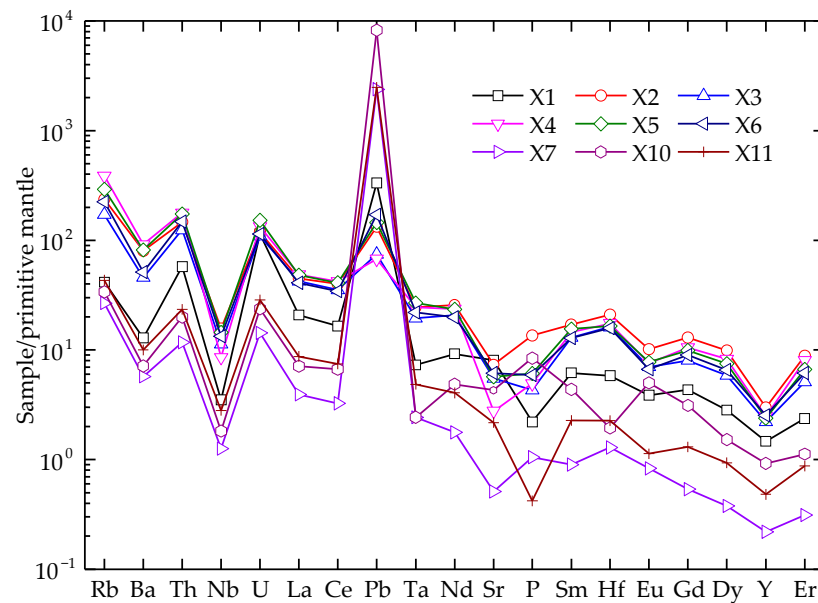


Figure 6. Primitive mantle-normalized trace element distribution patterns of ore from Xiaojiashan gold deposit.

5.2. Sulfur Isotope Compositions

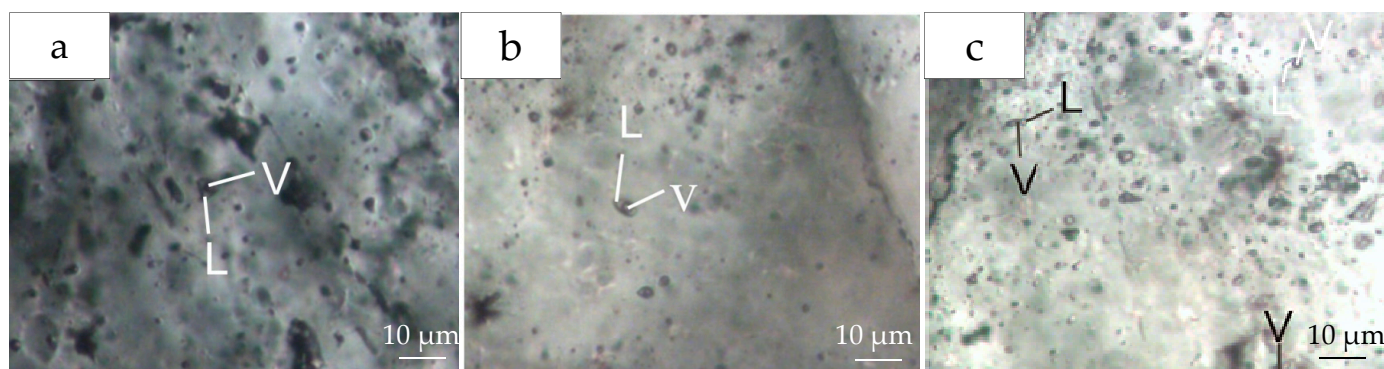
The sulfur isotope compositions of the pyrite samples from the Xiaojiashan deposit in different metallogenic stages and those from the Lengjiaxi Group are presented in Table 3. The $\delta^{34}\text{S}_{\text{VCDT}}$ values of the ore samples ranged from -3.1 to -8.0% . It is also shown in Table 3 that the sulfur isotope composition of pyrite from the ore samples X1–X11 were similar to the compositions of the samples from the Yanlinsi gold deposit (-10.34 ~ $+6.04$ [21,22]), the Zhengchong deposit (-8.9 ~ -0.1 [14]), and the Lengjiaxi Group in this area (-13.10 to -5.93% [13,21,40]).

Table 3. Sulfur isotopic compositions of pyrite from Xiaojiashan gold deposit (‰).

Sample	$\delta^{34}\text{S}_{\text{VCDT}}$	Sources	Sample	$\delta^{34}\text{S}_{\text{VCDT}}$	Sources	
X1	−8.0	This study	Pt ₂	−13.10~−6.26	[21]	
X3	−6.9		Yanlinsi	−5.73		
X5	−7.1			−4.57		
X7	−5.0		Xiaojiashan	−33.3~−0.99		[18]
X10	−3.1			−5.25~−2.05		[28]
X11	−7.6		Yanlinsi	−10.34~+6.12		[22]
Pt ₂	−10.4	[40]	Zhengchong	−8.9~−0.1	[14]	
Pt ₂	−12.56~−5.93	[13]				

5.3. Fluid Inclusion Microthermometry

Figures 3 and 7 show some microphotographs of polished slides of samples of the quartz from the Xiaojiashan deposit. Veinlets and veins hosted by the quartz of ore zones, and the fluid inclusions in quartz are distinguishably different quartz generations. To summarize the fluid inclusion study results: the fluid inclusions [41] in the quartz were difficult to study due to their small size (mostly 4.0–6.5 μm), they were all composed of vapor–liquid two–phase and liquid-rich fluid inclusions at room temperature, with the vapor phase accounting for 5–40 vol.% (mostly 20–30 vol.%) (Appendix A, Table 4). The shapes of the inclusions were nearly circular and elliptical, slightly rectangular, triangular, and diamond, as well as rather irregular.

**Figure 7.** Photomicrograph of fluid inclusions in quartz from Stages I (a), II (b), and III (c) in Xiaojiashan gold deposit.**Table 4.** Temperature of fluid inclusions in Xiaojiashan gold deposit.

Stage	No.	Size (μm)	Vapor (%)	Th ($^{\circ}\text{C}$)	Tm ($^{\circ}\text{C}$)	Ti ($^{\circ}\text{C}$)	Salinity (wt%) NaCl
I	X1	4.0–8.0	10–45	186–332	−6.8–−1.9	−22–−20	3.2–10.2
	X2	3.5–8.6	15–45	219–343	−6.4–−1.0	−23–−20	1.7–9.7
II	X3	4.0–7.5	10–30	169–314	−6.1–−0.5	−23–−20	0.8–9.3
	X5	3.8–9.0	5–40	167–296	−6.0–−0.8	−23–−20	1.4–9.2
	X7	4.5–7.5	10–40	183–302	−6.9–−2.3	−23–−20	3.8–10.3
	X8	4.0–8.6	5–45	137–288	−5.9–−1.3	−25–−20	2.2–9.0
	X9	4.6–10.7	5–35	184–295	−7.6–−2.4	−24–−20	4.0–11.2
III	X10	3.8–7.6	10–30	145–268	−7.6–−1.0	−23–−21	1.7–11.2
	X11	4.3–7.2	5–30	179–238	−7.8–−1.4	−25–−21	2.4–11.4
	X12	3.8–8.5	10–35	122–250	−5.4–−0.7	−25–−21	1.2–8.4

The fluid inclusions in Stage I were studied in veinlets and euhedral crystals, where they were distributed either in clusters or isolated, suggesting their primary nature. The

primary fluid inclusions in the samples were 3.5–8.6 μm (mostly 4.0–6.5 μm , as shown in Table 4, Figure 7a). They homogenized to liquid mostly in between 186 and 343 $^{\circ}\text{C}$, with an average of 274 $^{\circ}\text{C}$. The freezing temperature and the initial melting temperature of the inclusions were -6.8 – -1.0 $^{\circ}\text{C}$, and -23 – -20 $^{\circ}\text{C}$, respectively. These were around -21 $^{\circ}\text{C}$, suggesting that they were H_2O - NaCl system inclusions. The salinity of the primary inclusions was 1.7–10.2 wt.% NaCl based on T_m (-6.8 – -1.0 $^{\circ}\text{C}$) (Tables 4 and A1).

The fluid inclusions in Stage II (Figure 7b) were measured in veinlets and euhedral crystals. The primary inclusions were small (3.8–9.0 μm) and mostly occurred in rows along fractures; the secondary and pseudo-secondary inclusions are relatively rare. Their morphology, size, freezing temperature (-7.6 – -0.5 $^{\circ}\text{C}$) and initial melting temperature (-25 – -20 $^{\circ}\text{C}$) are similar to those of Stage I. However, their homogenization temperatures (137–314 $^{\circ}\text{C}$, with an average of 237 $^{\circ}\text{C}$) (Tables 4 and A2) were lower than those of most primary inclusions in Stage I.

The fluid inclusions in Stage III (Figure 7c) were studied in veinlets and veins. The proportion accounted for by the vapor phase (5–35 vol.%, mostly 15–25 vol.%) decreased (Tables 4 and A3). Their morphology, size (3.8–8.5 μm), freezing temperature (-7.8 – -0.7 $^{\circ}\text{C}$), and initial melting temperature (-25 – -21 $^{\circ}\text{C}$) were similar to those of Stages I and II. However, their homogenization temperatures (122–268 $^{\circ}\text{C}$, with an average of 198 $^{\circ}\text{C}$) were lower than those of most primary inclusions in Stages I and II.

The initial melting temperature of inclusions in Stages I, II, and III were around -21 $^{\circ}\text{C}$, suggesting that the ore-forming fluids comprised a H_2O - NaCl system. This suggests that the fluids involved in the hydrothermal episodes were similar.

The salinity of the fluid inclusions (ω , wt%) was calculated using Equation (1) [42].

$$\omega, \text{wt}\% = 1.78\theta - 0.0442\theta^2 + 0.000557\theta^3 \quad (1)$$

In Equation (1): θ is the depression of the freezing temperature in degrees Celsius.

The calculated values for the salinity of the fluid inclusions ranged from 5.6 to 11.2%, 4.2 to 11.2%, and 4.2 to 8.4% for Stages I, II, and III, respectively (Figure 8b).

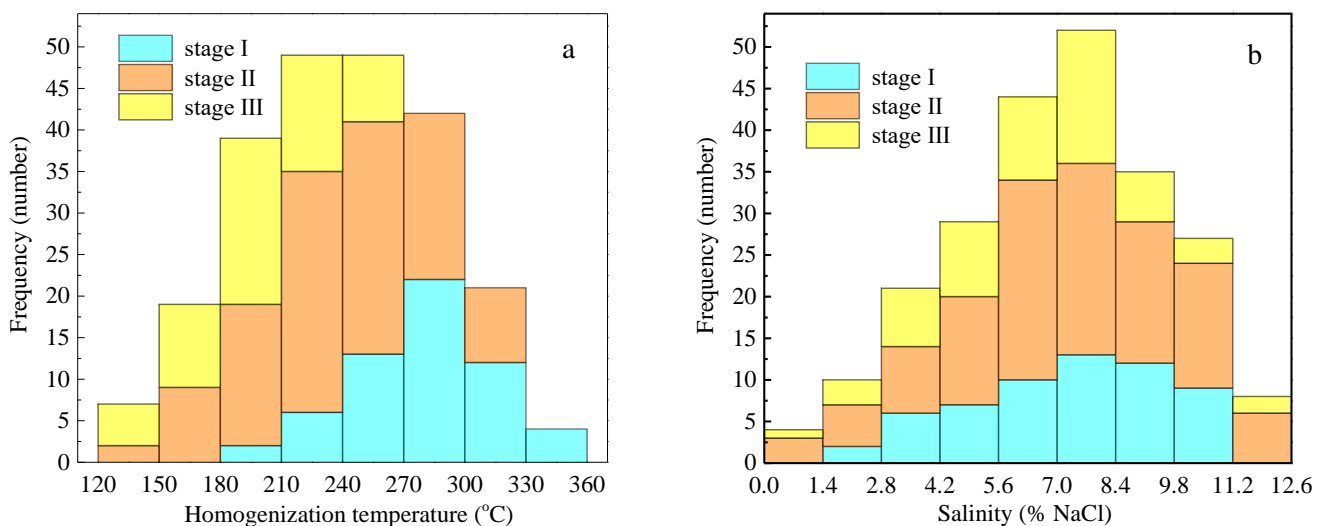


Figure 8. Histograms of homogenization temperature (a) and salinity (b) of fluid inclusions in Xiaojiashan gold deposit.

Figures 8 and 9 show that the temperature of the ore-forming fluid is highest during mineralization stage I, and the salinity of the ore-forming fluid is highest during mineralization stage II. In addition, a weak positive relationship between the homogenization temperatures and the salinity was identified for each stage of the fluid inclusions. The ore-forming fluid in this study may be a relatively hot and saline fluid, and the drop (from

Stages II to III) in salinity and temperature may have been caused by the addition of some colder and less saline fluid.

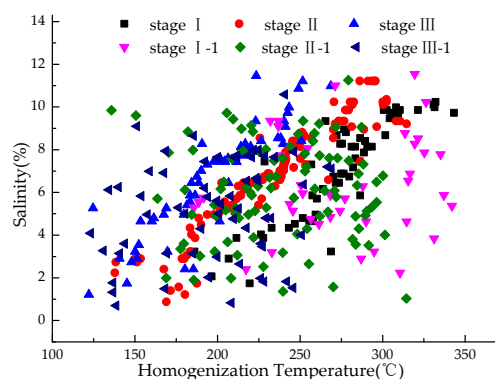


Figure 9. Diagram of temperature and salinity in Xiaojiashan gold deposit. The data of Stages I-1, II-1 and III-1 are from [30].

6. Discussion

6.1. Source of Ore-Forming Material

The contents of Au, Cu, Pb, Zn, As and Sb in the rocks of the Lengjiaxi Group in northeastern Hunan were 1.65, 1.68, 1.93, 1.70, 22.89 and 8.38 times the average concentrations of the upper crust, respectively (Table 5) [43,44]. The ore bodies of the Xiaojiashan gold deposit occur in the epi-metamorphic rocks of the Lengjiaxi Group. Fresh, unaltered, and mineralized samples of the Lengjiaxi Group's epi-metamorphic sandstone along with slate from the Yanlinsi ore section and its periphery were collected by Huang et al. [37]. In northeastern Hunan, Au, Cu, Zn and As were measured with varying degrees of enrichment. Both showed that the Lengjiaxi Formation is a rich source of Au. Figure 5 depicts the patterns of the chondrite-normalized REE distribution for the hosted rocks and ore, which were similar to those of the Lengjiaxi Group [39]. These features suggest that the Lengjiaxi Group provided a material source for mineralization.

Table 5. Abundance and parameters of some metallic elements in the Lengjiaxi Group and Xiaojiashan gold deposit in northeastern Hunan ($\omega(B)/\text{ppm}$, $\omega(\text{Au})/\text{ppb}$).

Position	No.	Au	Cu	Pb	Zn	As	Sb	Sources
① Northeastern Hunan	120	2.97	41.88	38.61	120.69	34.34	1.67	[43,44]
② Yanlinsi section	33	19.02	50.09	31.49	131.56	87.04	1.65	[37]
④ Upper crust		1.8	25	20	71	1.5	0.2	[45]
①/④		1.65	1.68	1.93	1.70	22.89	8.38	
②/①		6.40	1.20	0.82	1.09	2.53	0.99	

Original metamorphic rocks can be restored using rock-geochemical methods. The La/Yb-REE diagram is often used to discuss rock types and material sources due to its low level of errors and high accuracy [46,47]. The $\text{La}_{(N)}/\text{Yb}_{(N)}$ versus ΣREE diagram (Figure 10) demonstrates sample plots within the field of sedimentary rock and continental tholeiitic, signifying that the original rocks of Stages I and II and the hosted rocks were likely to have been sedimentary rock mixed with magmatic rock.

The $\delta^{34}\text{S}$ values of the sulfide can be approximately regarded as the $\delta^{34}\text{S}_{\Sigma}$ values of the ore-forming fluid when the mineral assemblage lacks sulfate [48]. The Xiaojiashan gold deposit possesses barren sulfate minerals, consisting of large amounts of pyrite, as well as small amounts of chalcopyrite, arsenopyrite, and galena. Therefore, the value of $\delta^{34}\text{S}$ in the pyrite is approximately equal to that in the ore-forming fluid.

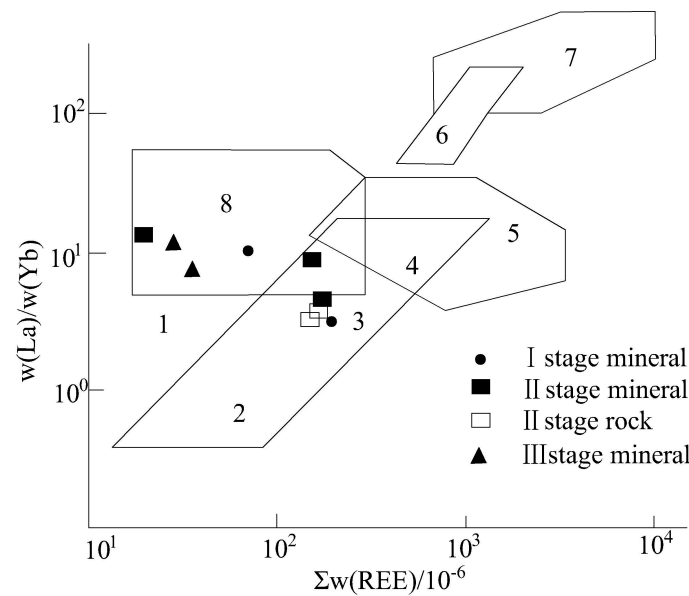


Figure 10. La/Yb-REE diagram for Xiaojiashan gold deposit (modified after [46]). 1. Chondrite; 2. Oceanic tholeiite; 3. Continental tholeiitic; 4. Alkalic basalt; 5. Granite; 6. Kimberlite; 7. Carbonatite; 8. Sedimentary rocks.

The $\delta^{34}\text{S}$ values of the pyrite in Stage I were low (-8.0‰), with similar values to the test samples from Xiaojiashan [18,28] and the Lengjiaxi Group in northeastern Hunan [13,21,40]. Furthermore, the pyrite in Stage I contained less ^{34}S than the magmatic sulfur ($\delta^{34}\text{S} = 0 \pm 3\text{‰}$) [49] from the same region (Figure 11 and Table 3). This indicates that the source of pyrite in Stage I was probably metamorphic sulfur, which is sourced from the metamorphism of sedimentary strata. The pyrite in Stage II and III had similar $\delta^{34}\text{S}$ values, which were also similar to the $\delta^{34}\text{S}$ values from Xiaojiashan (Figure 11 and Table 3) [18,28], Yanlinsi [21,22], and Zhengchong [14]. The pyrite in Stages II and III contained more ^{34}S than the Lengjiaxi Group in northeastern Hunan [13,21,40]. This indicates that there was an external magmatic sulfur source ($\delta^{34}\text{S} = 0 \pm 3\text{‰}$) [49], which may have migrated from the concealed plutons resulting from the magnetic anomaly beneath the Zhengchong–Xiaojiashan–Yanlinsi goldfield [18,37]. The trace element compositions and ratios of pyrite also suggest that the sulfur source and composition may have shifted from metamorphic (Stage I) to magmatic (Stage II) [18].

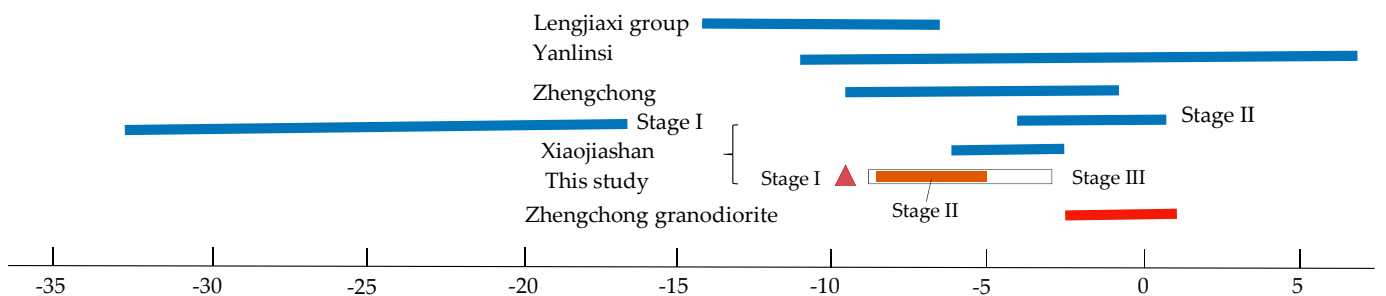


Figure 11. S isotopic compositions of pyrite and granodiorite from regional gold deposits. Sulfur isotope data of the Lengjiaxi Group [13,21,40], Yanlinsi [21,22], Zhengchong [14], Stages I and II [18], Xiaojiashan [28], and Zhengchong granodiorite [14] are shown for comparison.

It is thus estimated that the gold in Xiaojiashan was from the Lengjiaxi Formation, and that magmatic materials were added to the mineralization.

6.2. Fluid Evolution

It is known that fluid inclusions in minerals play an important role in the study of the ore-forming process, as these inclusions can reflect the properties of ore-forming fluid and invert the ore-forming process [50,51]. The vapor–liquid two-phase inclusions were found to develop in the hydrothermal quartz veins of the Xiaojiashan deposit, wherein no other inclusion types were discovered. The values of the homogenization temperature for the inclusions range mostly from 180 to 300 °C. This temperature range implies that the inclusions belonged to a hydrothermal solution with medium–low temperatures. The calculated salinity mainly varied from 4.2 to 11.2 % (wt% NaCl, eq), and no salt crystal was found in the inclusions, indicating a medium–low salinity for the ore-forming fluids. It is therefore considered that the ore-forming fluid of the Xiaojiashan gold deposit had a medium–low temperature and salinity range.

From the $\text{La}_{(N)}/\text{Yb}_{(N)}$ versus ΣREE diagram, the temperature and salinity diagram, and the $\delta^{34}\text{S}$ values of the pyrite, it can be shown that the ore-forming hydrothermal fluids were metamorphic–hydrothermal, with Au extracted from the strata during its migration in Stage I. According to the $\delta^{34}\text{S}$ values of the pyrite in Stages II and III, which contained a higher value of ^{34}S than that of the Lengjiayi Group in northeastern Hunan, it was found that the ore-forming hydrothermal fluids may have shifted to the magmatic stage (Stages II and III) from the metamorphic stage (Stage I). A similar fluid-evolution process in vein-hosted gold deposits has also been proposed in many orogenic gold deposits worldwide, such as the gold deposit in northeastern Hunan, China [13] and the Lac Herbin deposit in Canada [52].

7. Conclusions

The following conclusions were reached from the evaluation and discussion of the results obtained from the present work:

- (1) The Lengjiayi Group and magmatic components provided the ore-forming materials.
- (2) The ore-forming hydrothermal fluids of the Xiaojiashan gold deposit were metamorphic hydrothermal in Stage I, which may have been derived from the metamorphism of the strata, and then shifted to magmatic–hydrothermal in Stages II and III. For the Xiaojiashan gold deposit, the temperature and salinity of the ore-forming fluids were at a medium–low level.
- (3) The temperature and salinity of the ore-forming fluid decreased during the metallogenic epoch, which might have been a result of the gradually reduced ore-forming materials and mineralization, along with the addition of groundwater.

Author Contributions: Fieldwork: D.H. and S.L.; fluid inclusions microthermometry: D.H., S.L. and L.L.; writing—original draft preparation: D.H. and C.H.; writing—review and editing: H.Q. and B.T.; funding acquisition, L.L., C.H. and H.Q. All authors have read and agreed to the published version of the manuscript.

Funding: This study was supported by National Key R&D Program of China (2022YFC3702300), Natural Science Foundation of China (NO. 52004207, 51904225 and 51904224), Science and Technology Program of Shaanxi (2020JQ-748), Scientific Research Program funded by Xi’an Science and Technology Bureau (22GXFW0064), Scientific Research Project of Youth Team for Innovation of Construction Science of Shaanxi Provincial Department of Education (No. 21JP077) and Education Program of Shaanxi (21JK0766).

Acknowledgments: Authors are highly indebted to Qixing Yang, retired from The Division of Minerals and Metallurgical Engineering in Department of Civil, Environmental and Natural resources engineering at Luleå University of Technology, in Luleå, Sweden for proofreading the manuscript and providing some suggests regarding the language improvement.

Conflicts of Interest: The authors declare no conflict of interest.

Appendix A

Table A1. Microthermometry results of primary fluid inclusions in Stage I of Xiaojiashan gold deposit.

No.	Host Mineral	Size (μm)	Vapor (%)	Th ($^{\circ}\text{C}$)	Tm ($^{\circ}\text{C}$)	Ti ($^{\circ}\text{C}$)	Salinity (wt% NaCl eq)
X1	Qz	7.5	40	186	-1.9	-20	3.2
	Qz	5.8	35	196	-1.2	-22	2.0
	Qz	8.0	40	243	-2.6	-20	4.3
	Qz	4.8	30	206	-1.7	-22	2.9
	Qz	6.2	35	257	-3.6	-21	5.8
	Qz	7.8	45	251	-2.9	-20	4.8
	Qz	4.8	25	232	-2.6	-20	4.3
	Qz	5.5	20	227	-2.3	-21	3.8
	Qz	6.4	30	257	-2.8	-20	4.6
	Qz	5.7	35	277	-5.7	-21	8.8
	Qz	5.8	25	286	-4.7	-22	7.4
	Qz	6.1	20	332	-6.8	-20	10.2
	Qz	5.4	25	331	-6.6	-21	9.9
	Qz	5.5	30	330	-6.7	-22	10.1
	Qz	5.2	30	288	-5.0	-20	7.8
	Qz	6.1	25	211	-2.3	-22	3.8
	Qz	6.4	15	273	-4.0	-21	6.4
	Qz	6.1	20	274	-4.3	-22	6.8
	Qz	5.7	30	283	-5.2	-20	8.1
	Qz	4.5	10	293	-5.2	-21	8.1
Qz	4.0	25	276	-4.3	-22	6.8	
Qz	4.3	20	279	-4.2	-20	6.7	
X2	Qz	7.6	30	219	-1.0	-23	1.7
	Qz	6.8	35	246	-2.4	-22	4.5
	Qz	8.2	40	226	-2.4	-20	4.0
	Qz	6.3	20	289	-5.4	-22	8.4
	Qz	5.8	30	290	-5.2	-21	8.1
	Qz	5.5	20	259	-3.0	-20	4.9
	Qz	4.2	25	286	-5.5	-23	8.5
	Qz	8.6	30	276	-5.8	-22	8.9
	Qz	7.7	35	263	-3.8	-21	6.1
	Qz	7.2	30	270	-4.2	-20	6.7
	Qz	6.7	25	255	-2.8	-22	4.6
	Qz	6.4	30	282	-4.5	-21	7.1
	Qz	5.8	20	283	-4.8	-23	7.5
	Qz	6.8	15	260	-3.5	-20	5.7
	Qz	5.7	30	271	-4.0	-22	6.4
	Qz	4.3	25	343	-6.4	-21	9.7
	Qz	4.2	45	281	-5.2	-20	8.1
	Qz	3.9	35	300	-6.5	-21	9.8
	Qz	3.5	30	321	-6.5	-22	9.8
	Qz	6.7	35	275	-5.3	-21	8.2
	Qz	6.5	40	301	-5.6	-20	8.6
	Qz	6.9	30	304	-6.2	-22	9.4
	Qz	5.2	35	305	-6.4	-20	9.7
	Qz	6.4	30	306	-6.3	-21	9.6
	Qz	5.7	20	308	-6.6	-22	9.9
Qz	6.2	35	309	-6.4	-22	9.7	
Qz	6.0	30	309	-6.3	-23	9.6	
Qz	6.1	25	310	-6.5	-20	9.8	
Qz	5.3	20	302	-6.5	-21	9.8	

Table A1. Cont.

No.	Host Mineral	Size (μm)	Vapor (%)	Th ($^{\circ}\text{C}$)	Tm ($^{\circ}\text{C}$)	Ti ($^{\circ}\text{C}$)	Salinity (wt% NaCl eq)
X1'	Qz	4.3	10	286	−3.6		5.8
	Qz	6.2	10	268	−1.9	−22	3.2
	Qz	4.6	15	274	−5.3		8.2
	Qz	4.9	15	272	−5.6	−21	8.6
	Qz	5.1	10	228	−4.7		7.4
	Qz	6.3	10	256	−4.6	−20	7.3
	Qz	5.0	10	265	−6.1		9.3

Table A2. Microthermometry results of primary fluid inclusions in Stage II of Xiaojiashan gold deposit.

No.	Host Mineral	Size (μm)	Vapor (%)	Th ($^{\circ}\text{C}$)	Tm ($^{\circ}\text{C}$)	Ti ($^{\circ}\text{C}$)	Salinity (wt% NaCl eq)
X3	Qz	6.8	30	169	−0.5	−22	0.8
	Qz	5.9	25	180	−0.7	−20	1.2
	Qz	6.2	20	197	−3.0	−21	4.9
	Qz	7.3	30	273	−6.1	−20	9.3
	Qz	7.0	30	181	−1.8	−23	3.0
	Qz	6.8	20	201	−3.1	−20	5.1
	Qz	6.1	15	240	−4.6	−22	7.3
	Qz	5.7	20	308	−6.1	−21	9.3
	Qz	6.0	10	270	−5.5	−20	8.5
	Qz	5.8	30	310	−6.1	−23	9.3
	Qz	6.8	25	314	−6.0	−21	9.2
	Qz	7.5	20	241	−5.0	−23	7.8
	Qz	6.5	25	201	−3.2	−20	5.2
	Qz	6.2	20	231	−4.3	−22	6.8
	Qz	5.7	15	237	−4.4	−21	7.0
	Qz	4.8	20	229	−4.2	−22	6.7
	X5	Qz	4.5	15	238	−4.2	−22
Qz		6.1	25	252	−5.6	−20	8.6
Qz		5.8	20	242	−5.1	−21	8.0
Qz		4.8	30	167	−1.4	−22	2.4
Qz		4.6	30	171	−0.8	−23	1.4
Qz		4.0	25	271	−6.0	−20	9.2
Qz		6.3	35	176	−0.9	−21	1.5
Qz		6.9	20	228	−4.2	−23	6.7
Qz		4.5	10	187	−1.0	−22	1.7
Qz		3.8	20	230	−4.3	−20	6.8
Qz		4.3	25	296	−5.9	−23	9.0
Qz		8.4	20	239	−4.4	−21	7.0
Qz		9.0	25	204	−3.4	−22	5.5
Qz		8.1	25	230	−4.2	−23	6.7
Qz		6.7	30	245	−5.4	−20	8.4
Qz		6.9	20	247	−5.2	−23	8.1
Qz		5.6	35	216	−3.9	−22	6.3
Qz	4.8	40	240	−4.4	−20	7.0	
Qz	5.8	20	193	−3.0	−21	4.9	
Qz	6.2	25	225	−4.1	−23	6.5	
Qz	5.1	20	251	−5.7	−22	8.8	

Table A2. Cont.

No.	Host Mineral	Size (μm)	Vapor (%)	Th ($^{\circ}\text{C}$)	Tm ($^{\circ}\text{C}$)	Ti ($^{\circ}\text{C}$)	Salinity (wt% NaCl eq)
X7	Qz	6.2	20	240	−4.7	−20	7.4
	Qz	5.8	20	183	−2.6	−24	4.3
	Qz	5.4	25	186	−2.3	−21	3.8
	Qz	4.5	20	302	−6.9	−23	10.3
	Qz	5.5	25	302	−6.8	−21	10.2
	Qz	7.2	20	282	−6.8	−24	10.2
	Qz	6.5	25	239	−4.5	−20	7.1
	Qz	5.4	20	300	−6.8	−21	10.2
	Qz	5.1	15	300	−6.7	−22	10.1
	Qz	4.5	10	301	−6.8	−20	10.2
	Qz	7.5	25	190	−2.7	−24	4.4
	Qz	7.0	20	215	−4.0	−21	6.4
	Qz	6.8	35	278	−6.5	−22	9.8
	Qz	6.4	40	207	−3.2	−23	5.2
	Qz	5.7	20	250	−5.5	−24	8.5
	Qz	5.3	20	208	−3.3	−20	5.4
	Qz	6.1	30	214	−3.6	−24	5.8
	Qz	5.7	25	281	−6.7	−21	10.1
	Qz	6.3	20	216	−3.8	−22	6.1
	X8	Qz	5.8	25	244	−5.2	−24
Qz		6.0	20	279	−6.5	−24	9.8
Qz		5.7	20	280	−6.8	−20	10.2
Qz		6.8	25	240	−4.5	−20	7.1
Qz		5.9	25	276	−6.1	−22	9.3
Qz		6.7	15	150	−1.7	−21	2.9
Qz		7.4	10	137	−1.3	−24	2.2
Qz		6.4	20	183	−1.9	−20	3.2
Qz		5.8	5	138	−1.6	−20	2.7
Qz		4.0	20	151	−1.6	−22	2.7
Qz		4.5	25	178	−1.7	−21	2.9
Qz		8.4	30	153	−1.7	−23	2.9
Qz		8.1	20	218	−3.9	−20	6.3
Qz		8.6	35	288	−5.8	−20	8.9
Qz		6.5	45	281	−5.9	−21	9.0
Qz		6.1	20	220	−4.0	−24	6.4
Qz		7.4	25	241	−5.0	−22	7.8
Qz		6.8	30	223	−4.0	−25	6.4
Qz		5.7	20	227	−4.1	−23	6.5
X9		Qz	7.9	30	243	−5.2	−21
	Qz	7.0	25	246	−5.4	−22	8.4
	Qz	6.8	30	256	−5.5	−20	8.5
	Qz	6.4	35	248	−5.3	−20	8.2
	Qz	5.8	30	249	−5.4	−22	8.4
	Qz	6.1	25	270	−5.8	−21	8.9
	Qz	7.2	20	188	−2.9	−23	4.8
	Qz	6.5	15	286	−7.6	−24	11.2
	Qz	6.2	25	209	−3.3	−21	5.4
	Qz	5.7	10	184	−2.4	−24	4.0
	Qz	4.6	5	211	−3.5	−20	5.7
	Qz	6.4	20	213	−3.6	−22	5.8
Qz	6.9	25	295	−7.6	−21	11.2	
Qz	7.2	20	270	−6.8	−20	10.2	
Qz	6.4	30	293	−7.6	−24	11.2	
Qz	5.7	35	291	−7.6	−22	11.2	
Qz	6.5	30	294	−7.6	−23	11.2	
Qz	5.8	25	240	−4.6	−20	7.3	
Qz	6.1	20	241	−4.7	−21	7.4	

Table A2. Cont.

No.	Host Mineral	Size (μm)	Vapor (%)	Th ($^{\circ}\text{C}$)	Tm ($^{\circ}\text{C}$)	Ti ($^{\circ}\text{C}$)	Salinity (wt% NaCl eq)
	Qz	8.7	15	241	−4.8	−23	7.5
	Qz	10.7	20	250	−5.2	−24	8.1
	Qz	7.2	15	273	−6.1	−21	9.3
	Qz	6.8	20	250	−5.5	−23	8.5
	Qz	6.4	25	277	−6.5	−20	9.8
	Qz	5.9	30	251	−5.5	−24	8.5
	Qz	6.1	25	275	−6.1	−21	9.3
	Qz	4.6	15	286	−4.7		7.4
	Qz	5.7	10	253	−4.6	−20	7.3
X3'	Qz	5.1	15	267	−4.1		6.5
	Qz	6.2	20	250	−4.8	−22	7.5
	Qz	5.4	10	224	−3.3		5.4
	Qz	6.4	15	234	−3.9	−21	6.3
	Qz	5.7	10	212	−3.9		6.3
	Qz	5.3	10	246	−4.5		7.1
	Qz	4.1	15	226	−3.5		5.7
X5'	Qz	6.5	5	237	−4.1	−20	6.5
	Qz	4.7	20	179	−1.7		2.9
	Qz	8.3	15	202	−4.0	−22	6.4
	Qz	6.2	10	225	−5.5	−23	8.5

Table A3. Microthermometry results of primary fluid inclusions in Stage III of Xiaojashan gold deposit.

No.	Host Mineral	Size (μm)	Vapor (%)	Th ($^{\circ}\text{C}$)	Tm ($^{\circ}\text{C}$)	Ti ($^{\circ}\text{C}$)	Salinity (wt% NaCl eq)
	Qz	5.7	25	190	−4.4	−21	7.0
	Qz	6.4	15	161	−2.9	−22	4.8
	Qz	7.1	10	145	−1.0	−22	1.7
	Qz	6.8	20	151	−1.7	−23	2.9
	Qz	6.5	20	251	−7.6	−21	11.2
	Qz	4.6	25	243	−6.6	−23	9.9
	Qz	4.2	20	249	−7.3	−22	10.8
X10	Qz	7.0	25	268	−7.4	−23	10.9
	Qz	6.7	20	240	−6.1	−23	9.3
	Qz	4.8	25	216	−5.1	−23	8.0
	Qz	7.6	15	193	−4.6	−22	7.3
	Qz	6.6	30	241	−5.9	−23	9.0
	Qz	5.8	25	242	−6.4	−23	9.7
	Qz	4.7	25	188	−4.0	−21	6.4
	Qz	6.1	25	201	−4.8	−23	7.5
	Qz	5.4	20	236	−5.5	−23	8.5
	Qz	6.5	25	180	−1.4	−22	2.4
	Qz	5.7	30	179	−3.0	−24	4.9
	Qz	4.5	25	223	−7.8	−24	11.4
	Qz	6.2	30	238	−5.5	−23	8.5
	Qz	7.0	20	181	−3.3	−25	5.4
	Qz	5.2	10	183	−3.4	−23	5.5
X11	Qz	4.8	5	201	−4.7	−21	7.4
	Qz	4.3	20	184	−4.0	−23	6.4
	Qz	7.2	25	186	−3.6	−22	5.8
	Qz	6.4	20	211	−3.8	−23	7.4
	Qz	6.1	20	213	−5.0	−21	7.8
	Qz	5.8	15	204	−4.7	−21	7.4
	Qz	4.6	20	226	−5.4	−23	8.4
	Qz	5.1	25	206	−4.8	−21	7.5
	Qz	4.9	20	197	−4.7	−23	7.4

Table A3. Cont.

No.	Host Mineral	Size (µm)	Vapor (%)	Th (°C)	Tm (°C)	Ti (°C)	Salinity (wt% NaCl eq)
X12	Qz	5.2	25	150	−1.9	−24	3.2
	Qz	8.0	15	140	−1.7	−24	2.9
	Qz	7.6	20	147	−1.6	−23	2.7
	Qz	8.5	10	124	−3.2	−22	5.2
	Qz	7.8	20	122	−0.7	−21	1.2
	Qz	8.0	30	214	−5.2	−23	8.1
	Qz	5.2	35	204	−4.7	−24	7.4
	Qz	3.8	20	215	−4.9	−21	7.7
	Qz	6.4	15	160	−2.8	−23	4.6
	Qz	5.4	20	218	−5.1	−22	8.0
	Qz	6.2	25	153	−2.8	−21	4.6
	Qz	7.1	30	169	−3.2	−24	5.2
	Qz	6.7	20	152	−2.1	−25	3.5
	Qz	5.8	25	167	−3.0	−23	4.9
	Qz	5.3	20	250	−5.4	−21	8.4
	Qz	6.4	15	183	−3.6	−24	5.8
	Qz	6.2	20	239	−5.3	−25	8.2
	Qz	5.4	15	220	−5.2	−21	8.1
	Qz	5.2	20	187	−4.2	−25	6.7
X10'	Qz	4.1	20	185	−1.4		2.4
	Qz	6.4	15	169	−1.9		3.2
	Qz	5.1	10	206	−4.0		6.4
	Qz	5.3	15	190	−5.3	−22	8.2
	Qz	4.3	10	216	−5.3		8.2
	Qz	5.6	20	223	−6.1		9.3
	Qz	4.8	15	201	−2.8		4.6

References

- Myint, A.Z.; Wagner, T.; Fusswinkel, T. Calcite trace element geochemistry of Au deposits in the Singu-Tabekkyin Gold District, Myanmar: Implications for the sources of ore-forming fluids. *Ore Geol. Rev.* **2022**, *145*, 104892. [\[CrossRef\]](#)
- Ye, X.; Bai, F. Spectral Characteristics, Rare Earth Elements, and Ore-Forming Fluid Constrains on the Origin of Fluorite Deposit in Nanlishu, Jilin Province, China. *Minerals* **2022**, *12*, 1195. [\[CrossRef\]](#)
- Prasolov, E.M.; Sergeev, S.A.; Belyatsky, B.V.; Bogomolov, E.S.; Gruzdov, K.A.; Kapitonov, I.N.; Krymsky, R.S.; Khalenev, V.O. Isotopic Systematics of He, Ar, S, Cu, Ni, Re, Os, Pb, U, Sm, Nd, Rb, Sr, Lu, and Hf in the Rocks and Ores of the Norilsk Deposits. *Geochem. Int.* **2018**, *56*, 50–69. [\[CrossRef\]](#)
- Kraemer, D.; Viehmann, S.; Banks, D.; Sumoondur, A.; Koeberl, C.; Bau, M. Regional variations in fluid formation and metal sources in MVT mineralization in the Pennine Orefield, UK: Implications from rare earth element and yttrium distribution, Sr-Nd isotopes and fluid inclusion compositions of hydrothermal vein fluorites. *Ore Geol. Rev.* **2019**, *107*, 960–972. [\[CrossRef\]](#)
- Chi, G.; Diamond, L.W.; Lu, H.; Lai, J.; Chu, H. Common Problems and Pitfalls in Fluid Inclusion Study: A Review and Discussion. *Minerals* **2021**, *11*, 7. [\[CrossRef\]](#)
- Deng, J.; Wang, Q.F. Gold mineralization in China: Metallogenic provinces, deposit types and tectonic framework. *Gondwana Res.* **2016**, *36*, 219–274. [\[CrossRef\]](#)
- Duan, L.A.; Gu, H.L.; Deng, J.H.; Yang, X.Y. Geological study and significance of typical gold deposits in eastern Qinzhou-Hangzhou metallogenic belt: Constraint from Tianjingshan gold deposit in south Anhui Province. *J. Geochem. Explor.* **2018**, *190*, 87–108. [\[CrossRef\]](#)
- Huang, J.Z.; Sun, J.; Zhou, C.; Lu, W.; Xiao, R.; Guo, A.; Huang, G.F.; Tan, S.; Wei, H.T. Metallogenic Regularity and Resource Potential of Gold Deposits of Hunan Area in the Jiangnan Orogenic Belt, South China. *Acta Geosci. Sin.* **2020**, *41*, 230–252. [\[CrossRef\]](#)
- Mao, J.W.; Hua, R.M.; Li, X.B. A Preliminary study of large-scale metallogenesis and large clusters of mineral deposits. *Miner. Depos.* **1999**, *18*, 291–299. [\[CrossRef\]](#)
- Wen, Z.L.; Deng, T.; Dong, G.J.; Zou, F.H.; Xu, D.R.; Wang, Z.L.; Lin, G.; Chen, G.W. Characteristics of Ore-controlling Structures of Wangu Gold Deposit in Northeastern Hunan Province. *Geotecton. Et Metallog.* **2016**, *40*, 281–294. [\[CrossRef\]](#)
- Wang, J.Q.; Shu, L.S.; Santosh, M. Petrogenesis and tectonic evolution of Lianyungshan complex, South China: Insights on Neoproterozoic and late Mesozoic tectonic evolution of the central Jiangnan Orogen. *Gondwana Res.* **2016**, *39*, 114–130. [\[CrossRef\]](#)

12. Sun, S.C.; Yang, L.Q.; Zhang, L.; Olin, P.; Gao, X.; Li, R.H.; Wang, J.Y.; Li, Z.Q.; Zhang, F.; Wen, T. In-situ trace elements on pyrite and arsenopyrite of the Zhengchong gold deposit, Jiangnan Orogen: Insights for the mineralization mechanism. *Ore Geol. Rev.* **2020**, *122*, 1–28. [[CrossRef](#)]
13. Xu, D.R.; Deng, T.; Chi, G.X.; Wang, Z.L.; Zou, F.H.; Zhang, J.L.; Zou, S.H. Gold mineralization in the Jiangnan Orogenic Belt of South China: Geological, geochemical and geochronological characteristics, ore deposit-type and geodynamic setting. *Ore Geol. Rev.* **2017**, *88*, 565–618. [[CrossRef](#)]
14. Liu, Q.Q.; Shao, Y.J.; Chen, M.; Algeo, T.J.; Li, H.; Dick, J.M.; Wang, C.; Wang, W.S.; Li, Z.Q.; Liu, Z.F. Insights into the genesis of orogenic gold deposits from the Zhengchong gold field, northeastern Hunan Province, China. *Ore Geol. Rev.* **2019**, *105*, 337–355. [[CrossRef](#)]
15. Zhang, L.; Groves, D.I.; Yang, L.Q.; Sun, S.C.; Weinberg, R.F.; Wang, J.Y.; Wu, S.G.; Gao, L.; Yuan, L.L.; Li, R.H. Utilization of pre-existing competent and barren quartz veins as hosts to later orogenic gold ores at Huangjindong gold deposit, Jiangnan Orogen, southern China. *Miner. Depos.* **2020**, *55*, 363–380. [[CrossRef](#)]
16. Peng, B.; Frei, R. Nd–Sr–Pb isotopic constraints on metal and fluid sources in W–Sb–Au mineralization at Woxi and Liaojiaping (Western Hunan, China). *Miner. Depos.* **2004**, *39*, 313–327. [[CrossRef](#)]
17. Li, W.; Cook, N.J.; Xie, G.Q.; Mao, J.W.; Ciobanu, C.L.; Fu, B. Complementary Textural, Trace Element, and Isotopic Analyses of Sulfides Constrain Ore-Forming Processes for the Slate-Hosted Yuhengtang Au Deposit, South China. *Econ. Geol.* **2021**, *116*, 1825–1848. [[CrossRef](#)]
18. Tan, H.J.; Shao, Y.J.; Liu, Q.Q.; Zhang, Y.; Feng, Y.Z.; Zhang, Y.C.; Shah, S.A. Textures, trace element geochemistry and in-situ sulfur isotopes of pyrite from the Xiaojiashan gold deposit, Jiangnan Orogen: Implications for ore genesis. *Ore Geol. Rev.* **2022**, *144*, 104843. [[CrossRef](#)]
19. Gu, X.X.; Schulz, O.; Vavtar, F.; Liu, J.M.; Zheng, M.H.; Fu, S.H. Rare earth element geochemistry of the Woxi W–Sb–Au deposit, Hunan Province, South China. *Ore Geol. Rev.* **2007**, *31*, 319–336. [[CrossRef](#)]
20. Gu, X.X.; Zhang, Y.M.; Schulz, O.; Vavtar, F.; Liu, J.M.; Zheng, M.H.; Zheng, L. The Woxi W–Sb–Au deposit in Hunan, South China: An example of Late Proterozoic sedimentary exhalative (SEDEX) mineralization. *J. Asian Earth Sci.* **2012**, *57*, 54–75. [[CrossRef](#)]
21. Liu, L.M.; Peng, S.L.; Wu, Y.Z. Features of metallogenic-tectonics and mechanism of tectonic-metallization for vein-type gold deposits in the north-eastern Hunan, China. *Geotecton. Et Metallog.* **1997**, *21*, 197–204, (In Chinese, with English abstract).
22. Dong, G.J.; Xu, D.R.; Wang, L.; Chen, G.H.; He, Z.L.; Fu, G.G.; Wu, J.; Wang, Z.L. Determination of mineralizing ages on gold ore deposits in the eastern Hunan province, south China and isotopic tracking on ore-forming fluids—Re-discussing gold ore deposit type. *Geotecton. Et Metallog.* **2008**, *32*, 482–491. [[CrossRef](#)]
23. Hunan, G.S.I. *Work Report on Detailed Investigation of Xiaojiashan Gold Deposit, Liling*; Private communication; Hunan, G.S.I.: Changsha, China, 2015; (internal report in Chinese).
24. Xie, H.Y.; Mao, W.H.; Hu, S.M.; Zhang, W.D. Geological characteristics and prospecting prospect of Xiaojiashan gold deposit. *Land Resour. Her.* **2007**, *34*–37. (In Chinese) [[CrossRef](#)]
25. Liu, S.L.; Xu, H.; Wen, T.; Cao, W.; Zhang, Q. Ore-controlling regularities and metallogenic prediction of Xiaojiashan gold deposits, northeastern Hunan. *Miner. Explor.* **2016**, *7*, 445–449. [[CrossRef](#)]
26. Zhang, C.G.; Zha, D.H.; Liu, M.H.; Zhou, H.S.; Shi, X.J.; Yan, Y.T.; Huang, K. Gold Element Fractal Characteristics and Geological Significance of Xiaojiashan Gold Deposit. *J. Xinyang Norm. Univ. (Nat. Sci. Ed.)* **2019**, *32*, 421–425. [[CrossRef](#)]
27. Zhang, Y.C.; Shao, Y.J.; Liu, Q.Q.; Zhang, X.; Zhan, Y.D.; Wang, C.; Wu, H.H.; Sun, J. Pyrite textures, trace element and sulfur isotopes of Yanlinsi slate-hosted deposit in the Jiangnan Orogen, South China: Implications for gold mineralization processes. *Ore Geol. Rev.* **2022**, *148*, 105029. [[CrossRef](#)]
28. Jiang, X.X.; Li, J.; Zhao, T. Ore-forming Material Source of Xiaojiashan Gold Deposit of Northeastern Hunan. *Land Resour. Her.* **2016**, *13*, 1–7. [[CrossRef](#)]
29. Tao, S.L.; Lai, J.Q.; Song, W.G.; Zha, D.H. Geological characteristics and metallogenic conditions of Xiaojiashan gold deposit in Liling of Hunan. *Miner. Resour. Geol.* **2015**, *29*, 195–202, (In Chinese with English abstract).
30. Lin, S. Research on Mineralizing Fluid Geochemistry Characteristics of Xiaojiashan Gold Deposit. *South. Met.* **2020**, *6*, 27–33. [[CrossRef](#)]
31. Xie, G.Q.; Mao, J.W.; Li, W.; Fu, B.; Zhang, Z.Y. Granite-related Yangjiashan tungsten deposit, southern China. *Miner. Depos.* **2019**, *54*, 67–80. [[CrossRef](#)]
32. Zhou, Y.Q.; Xu, D.R.; Dong, G.J.; Chi, G.X.; Deng, T.; Cai, J.X.; Ning, J.T.; Wang, Z.L. The role of structural reactivation for gold mineralization in northeastern Hunan Province, South China. *J. Struct. Geol.* **2021**, *145*, 104306. [[CrossRef](#)]
33. Liu, Y.; Zhang, L.; Sun, S.C.; Qi, P.; Wu, S.G.; Gao, L. Mineralization mechanism of Yangshanzhuang gold deposit, northeastern Hunan Province. *Acta Petrol. Sin.* **2017**, *33*, 2273–2284, (In Chinese with English abstract).
34. Jia, B.B.; Peng, H.Q.; Chen, J. *Changsha of Regional Geological Survey Report in 1:250000*; Private communication; Geological Bureau of Hunan Province: Changsha, China, 2002; (internal report in Chinese)
35. Li, J.H.; Zhang, Y.Q.; Dong, S.W.; Mang, Z.L.; Li, Y. LA-MC-ICPMS Zircon U–Pb Geochronology of the Hongxiaqiao and Banshanpu Granitoids in Eastern Hunan Province and Its Geological Implications. *Acta Geosci. Sin.* **2015**, *36*, 187–196. [[CrossRef](#)]

36. Xu, D.R.; Deng, T.; Dong, G.J.; Ning, J.T.; Wang, Z.L.; Zhang, J.L.; Zou, F.H.; Zhou, Y.Q.; Chen, G.W.; Yu, D.S.; et al. Zircon U-Pb geochronological and geochemical characteristics of the Lianyungshan two-mica monzogranites in northeastern Hunan Province: Implications for petrogenesis and tectonic setting associated with polymetallic mineralization. *Earth Sci. Front.* **2017**, *24*, 104–122. [[CrossRef](#)]
37. Huang, C.; Fan, G.M.; Jiang, G.L.; Luo, L.; Xu, Z.L. Structural Ore-controlling Characteristics and Electron Spin Resonance Dating of the Yanlinsi Gold Deposit in Northeastern Hunan Province. *Geotecton. Et Metallog.* **2012**, *36*, 76–84. [[CrossRef](#)]
38. Sun, W.D.; William, F.M. Chemical and isotopic systematics of oceanic basalts: Implications for mantle composition and processes. *Geol. Soc. Lond. Spec. Publ.* **1989**, *42*, 313–345. [[CrossRef](#)]
39. Liu, L.M.; Peng, S.L.; Wu, Y.Z. Genetic features forming vein-type gold deposits in northeastern Hunan. *Geotecton. Et Metallog.* **1999**, *30*, 4–7, (In Chinese with English abstract)
40. Luo, X.L. Discussion on the material sources of gold deposits in Precambrian strata in Hunan. *J. Guilin Univ. Technol.* **1990**, *10*, 13–25.
41. Goldstein, R.H.; Reynolds, T.J. Systematics of Fluid Inclusions in Diagenetic Minerals. *Soc. Sediment. Geol. Short Course* **1994**, *31*, 199.
42. Hall, D.L.; Sterner, S.M.; Bodnar, R.J. Freezing point depression of NaCl-KCl-H₂O solution. *Econ. Geol.* **1988**, *83*, 197–202. [[CrossRef](#)]
43. Liu, Y.C. Geochemical signatures of the Huangjindong gold deposit. *Geol. Explor.* **1989**, *11*, 43–48, (In Chinese with English abstract)
44. Ma, D.S.; Liu, Y.J. Geochemical characteristics and genesis of strata bound gold deposits in Jiangnan gold metallogenic belt. *Sci. Sin.* **1991**, *4*, 424–433. (In Chinese)
45. Taylor, S.R.; McClenan, S.M. *The Continental Crust: Its Composition and Evolution*; Blackwell Scientific Publications: Oxford, UK, 1985; p. 46.
46. Allègre, C.; Minster, J.F. Quantitative models of trace element behavior in magmatic processes. *Earth Planet. Sci. Lett.* **1978**, *38*, 1–25. [[CrossRef](#)]
47. Taylor, S.R.; Mclennan, S.M. *The Composition and Evolution of the Continental Crust: Rare Earth Element Evidence from Sedimentary Rocks*; Phi. Trans. R. Soc.: London, UK, 1981; Volume 301, pp. 381–399.
48. Ohmoto, H.; Rye, R.O. Isotopes of sulfur and carbon. In *Geochemistry of Hydrother-Mal Ore Deposits*; Barnes, H.L., Ed.; John Wiley&Sons: Hoboken, NJ, USA, 1979; pp. 509–567.
49. Ohmoto, H. Systematics of Sulfur and Carbon Isotopes in Hydrothermal Ore Deposits. *Econ. Geol.* **1972**, *67*, 551–578. [[CrossRef](#)]
50. Ulrich, T.; Günther, D.; Heinrich, C.A. The evolution of a porphyry Cu-Au deposit, based on LA-ICP-MS analysis of fluid inclusions: Bajo de la Alumbrera, Argentina. *Econ. Geol.* **2001**, *96*, 1743–1774. [[CrossRef](#)]
51. Deng, J.; Yang, L.Q.; Gao, B.F.; Sun, Z.S.; Guo, C.Y.; Wang, Q.F.; Wang, J.P. Fluid evolution and metallogenic dynamics during tectonic regime transition: Example from the Jiapigou gold belt in northeast China. *Resour. Geol.* **2009**, *59*, 140–152. [[CrossRef](#)]
52. Rezeau, H.; Moritz, R.; Beaudoin, G. Formation of Archean batholith-hosted gold veins at the Lac Herbin deposit, Val-d’Or district, Canada: Mineralogical and fluid inclusion constraints. *Min. Depos.* **2017**, *52*, 421–442. [[CrossRef](#)]

Disclaimer/Publisher’s Note: The statements, opinions and data contained in all publications are solely those of the individual author(s) and contributor(s) and not of MDPI and/or the editor(s). MDPI and/or the editor(s) disclaim responsibility for any injury to people or property resulting from any ideas, methods, instructions or products referred to in the content.